# Towards a maintainable and high efficiency neutral beam system for future fusion reactors

A. Simonin, C. Blondel, W. Chaibi, C. Dechelle, C. Drag, E. Villedieu

# Towards a maintainable and high efficiency neutral beam system for future fusion reactors

**A. Simonin[1], C. Blondel[2] , W. Chaibi[3], C. Dechelle[1], C. Drag[2], E. Villedieu[1].**

[1] *CEA, IRFM, F-13108 St Paul lez Durance, France*
[2] *Laboratoire de Physique des plasmas, Centre national de la recherche scientifique, Sorbonne Université, Université Paris-Saclay, Observatoire de Paris, Ecole polytechnique, Institut polytechnique de Paris, route de Saclay, F-91128 Palaiseau cedex, France*
[3] *Laboratoire ARTEMIS-UMR CNRS 7250, Cote d'Azur Observatory, Nice, France*

*E-mail:* ***alain.simonin@cea.fr***

Received xxxxxx
Accepted for publication xxxxxx
Published xxxxxx

## Abstract

Achievement of an economic fusion reactor imposes a high level of unprecedented requirements for the Neutral Beam (NB) systems; the first one is the nuclear safety constraints which imposes prerequisite on the ease of access of all injector components to provide a preventive (and curative) maintenance by remote handling while maintaining reactor operation. In addition, the challenge is to develop high power injectors with very high wall-plug efficiency (above 60 %) able to operate in stable conditions over several months. There is a significant gap to bridge with respect to the present NB systems, which are handicapped by a low efficiency and by complex and long maintenance operations. Evidence that this injector concept does not offer adaptations to cope with the reactor requirements makes it clear that a new concept has to be addressed. An injector concept with modular sources at ground voltage is proposed. The concept makes remote maintenance of the injector components easier where each source module can be replaced by a new one without breaking the vacuum and affecting injector conditioning. With the grounded and modular ion source, photoneutralization associated with energy recovery appears as the best route capable of attaining the reactor requirements. This concept of maintainable NB system would provide a high heating power with a wall-plug efficiency above 70% and unprecedented features such as the capacity of producing temporal and spatial modulation of the beam power for a better control of the plasma stability. Up to now, photoneutralization feasibility studies already carried out on reduced-scale prototypes have not highlighted any showstoppers. Continuation of R&D in the years to come can pave the way towards the achievement of a first full-scale high power cavity in the 1 MW range, and to the realization of a multi-amperes (~10 A) thin blade-like D- beam.

Keywords: Fusion reactors, Neutral beams, Photoneutralization, Efficiency, RAMI, Remote handling.

## 1. Introduction

In line with the ITER machine project, which seeks to demonstrate the feasibility of fusion power, the purpose of current research and development is to pave the way for the industrial and commercial exploitation of a fusion reactor. The medium-term objective (2040-2050) is to implement a prototype for a quasi-industrial reactor (DEMO) [1] connected to the grid, with a substantial electrical power output in the order of 500 MWe. In the overall fusion strategy, the ITER machine is the

 

stage before the reactor, the goal being to explore and to study the physics and technology at a scale close to that of the reactor. The fusion power will however be moderated; numerically 500 MW of D-T fusion reactions in the plasma core are expected to last only 400 seconds, without electricity production.

The fusion reactor dedicated to electricity production will differ from the ITER machine in several aspects. It will have three or four times the D-T fusion reaction rate (~1.5 to 2 GW of D-T fusion reactions) leading to an unprecedented neutron load of 14 MeV [2], self-fuelling of the reactor with tritium [3], pulsed (pulse duration of 2 hours or more) or quasi stationary plasma operating times, and reactor exploitation over long periods. Achieving these operating conditions presents new technical challenges and introduces new nuclear security requirements to protect workers and the environment.

Production of such a high power D-T fusion over a long period of time will result in a substantial consumption of tritium: though there are just grams of tritium present at any one time in the reactor plasma, the estimated annual consumption for one reactor is in the order of tens of kilograms [3]. Tritium is the primary radioactive source in a fusion power plant. Due to diffusion and migration, it will be present in a lesser extent in the vacuum vessels connected to the tokamak chamber, namely in the neutral beam tanks.

Other radioactive sources are the materials activated by the fusion neutrons (14 MeV) and tritiated dust (estimated to be several hundred kg by a reactor's end-of-life [4]) resulting from the erosion of the reactor first wall by the plasma.

Consequently, the nuclear safety constraints result firstly in a series of containment barriers between the nuclear island, the workers and the environment, secondly in organisational arrangements (remote and robotic handling), and thirdly in personal protection provisions during daily operation of the reactor to avoid any exposure to radiation or chemical compounds (beryllium or dust).

To minimise the probability of failure, or accidents and their detrimental impacts on the safety and availability of the plant, each subsystem and its equipment is subject to a high prerequisite requirement of reliability. In this context, preventative maintenance measures aim to make it easy to replace or repair each component or system in the plant. High importance is placed on the design of the reactor and its subsystems, especially on the ease of access of essential components during inspections. This leads to an implementation of sophisticated engineering solutions using remote handling and robotization from their assembly and disassembly of components, to their transfer and storage in hot cells, all without affecting the plant's operation.

These new requirements are requested for reactors internal components as well as neutral beam systems, both of which must be designed to an unprecedented standard of reliability and availability in order to maintain and control the D-T fusion reactions in the plasma core over long operational periods.

Simulation of scenarios for pulsed or stationary plasma with generation of non-inductive current show that the ignition of D-T fusion reactions and the active control of the q-profile require additional heating power coupled to the plasma core, to the amount of 50 to 150 MW [5], a non-trivial amount compared to the electricity production of the plant (target 1 GWe). Thus, the development of high-efficiency heating systems (with wall-plug efficiency > 50 %) aiming to minimise the electrical power recirculated within the plant [6] is combined with the RAMI (Reliability, Accessibility, Maintainability, Inspectability) requirements and nuclear safety requirements. This is a significant technological and scientific gap to be bridged with respect to the present state of the art, as the efficiency of current NBI systems remains lower than 30%.

As a consequence, the compatibility of the present architecture of NBI systems with these new requirements appears highly debatable.

## 2. Agreement analysis of current conventional neutral beam systems with reactors requirements

Conventional neutral beamlines (ITER type [7]) are principally composed of a high voltage assembly comprising the ion source held at high voltage (-1 MV on ITER) and the accelerator, both connected and suspended under the tank vacuum to a -1 MV bushing (see Fig.1). Downstream of the accelerator, the injector includes an assembly of thermomechanical components at ground voltage: a gas neutraliser, a residual ion dump (RID) system and a beam target.

 

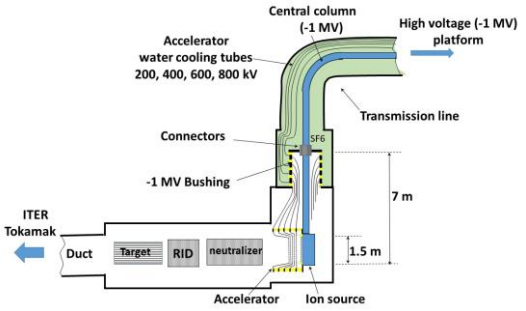


*Figure 1: Principle of a 1 MeV neutral beam system (ITER type) with source at high voltage (-1 MV).*

### *2.1 The Bushing [8-9]*

The bushing is a feedthrough at a very high voltage (-1 MV) situated between the transmission line under 5 bars of $SF_6$ and the source in the vacuum vessel. The transmission line is connected to the high voltage platform (-1 MV) containing all the power supplies of the source.

The bushing is composed of a stack of five insulators separated by metal shields, with a 200 kV potential difference between each shield, creating a voltage gradient between the grounded vacuum tank and the central column at -1 MV, which contains all the cables that supply the source plasma. Around 100 different connectors located in the bushing central column (-1MV) are required to ensure the continuity of the circuits between the transmission line (under $SF_6$) and the source (under vacuum). In the event of failure (HV breakdowns, arc, or loose contact), their inspection or repair cannot be handled remotely: the complete bushing will have to be replaced. This is an extensive operation leading to a long-term unavailability of the injector.

### *2.2 The negative ion source [10]*

The source is the second active and complex element of the injector. It relies on several sub-systems and power supplies installed on the high voltage (-1 MV) platform. They include cooling water, gas (hydrogen or deuterium), radio frequency power supply (800 kW, 1 MHz) for the eight Inductively Coupled Plasma (ICP) drivers, plasma diagnostics (probes, optical fibres, thermocouples), and various high current or high voltage electrical supplies, such as : “5000 A, 10 V, DC” to generate the transverse magnetic field filter”, or “5000 A, 15 V, DC” for the polarisation of the plasma grid, or “12 kV, 140 A, DC” for the polarisation of the extraction grid, or “150 V, 2 A, DC” for the caesium oven.

This results in a multitude of connectors and cables implemented within the bushing central column. Their proximity and inaccessibility is a source of trouble which could strongly impacts the injector overall reliability and availability.

### *2.3 The 1 MeV accelerator [11]*

It is a Multi-aperture Multi-Gap (MaMuG) system which consists of five accelerator stages between -1 MV (on the source level) and the last accelerating stage at the ground, with a potential difference of 200 kV between each stage. It is subject to a high level of thermomechanical stresses due to the power of the ion beam (40 A $D^-$ accelerated at 1 MeV, equivalent of 40 MW in DC) passing through 1280 accelerating channels (beamlets) of its acceleration grids. The gas injected in the source ($p_s$ ~0.3 Pa) and diffusing downstream in the accelerator leads to the stripping of the $D^-$ extra electron by means of collisions. The process leads to parasite particles ($e^-$, $D^+$, $D^0$) in the accelerating channel bombarding the accelerator grids and generating an electron multiplication by secondary electron emission. Simulations of these stray particles emission and trajectories [11-12] estimate the thermal load in the accelerator grids between 8 and 10 MW, consisting of 1 to 2 MW per stage. The active cooling and voltage bias (-800, -600, -400, -200 kV) of the acceleration grids is provided by water tubes crossing the different bushing stages.

### *2.4 The gas neutraliser*

It is a passive and thermomechanical element of the line at the ground potentiel. The optimal gas target density required to attain the maximum degree of neutralisation (~55%) for $D^-$ at 1 MeV is $n_{D2}$. $L_{neut}$ = 1.2 $10^{20}$ $m^{-2}$, where $n_{D2}$ ~ 4 $10^{19}$ $m^{-3}$ is the average gas density ($D_2$) along the neutralizer length ($L_{neut}$~3m). To avoid gas diffusing backwards in the accelerator and increasing the $D^-$ losses by stripping, the neutraliser is located 0.5 m away from the accelerator exit (see Fig.1) to favour the gas conductance towards the cryogenic pumps. As a consequence, wide openings in the neutraliser (10 cm width) are required to permit the beam to pass without interception, but, it leads to a substantial increase of the neutraliser gas conductance; indeed, around 80% of the amount of gas is injected into the neutraliser (only 20 % in the source).

### *2.5 The residual ion dump (RID)*

 

The RID at the exit of the neutraliser is also a thermomechanical element actively cooled with the purpose of intercepting residual ions (8 A of residual $D^+$ and 8 A of $D^-$ at 1 MeV), equivalent to 16 MW of continuous thermal load. The RID is connected to a high flow water cooling system and to an external power supply of ± 20 kV for the electrostatic deflection of the residual ions out from the neutral beam and their collection on electrodes.

### *2.6 Efficiency of the neutral beam line:*

Nominally, each beamline is expected to inject 17 MW of $D^0$ at 1 MeV into the plasma core. The wall plug efficiency (ratio of the neutral beam power coupled to the plasma core to the total electrical power consumed by the beamline) is evaluated at 30%. This low value results principally from the low rate of neutralisation ($\eta \sim 55\%$), absence of energy recovery from the residual ions (~16 MW lost) and the 10 MW thermal load (loss from stripping of $D^-$) in the accelerator.

Adapting an energy recovery system for the residual ions to this injector (with the ion source at -1 MV) [13] is of limited interest due to the additional complexity: this would require collecting ions ($D^+$ and $D^-$) at a high voltage (resp. +1MV and -1MV) involving two additional invasive bushings (at ±1 MV) and $SF_6$ transmission lines. In addition, these high voltage electrodes downstream to the neutralizer exit would drain charged particles extracted from the secondary plasma formed within the neutralizer cell.

### *2.7 Remote handling of the neutral beamline components:*

#### *2.7.1 Maintenance of the source, accelerator and caesium oven*

All intervention on the source or the accelerator takes place at atmospheric pressure after opening the rear flange of the vessel. During air exposure, adsorbates like hydrocarbons, water and dust cover the clean "bushing & accelerator" surfaces exposed to the high electric fields that significantly degrade the injector conditioning. Moreover, the caesium deposited on the internal walls of the source and the plasma grid will be oxidised by the air intake and will have to be washed and removed by water spray. Such maintenance impacts on the injector availability as restarting the injector and bringing it back up to its nominal (1 MeV) will require a long reconditioning of the plasma source, of the high voltage holding (-1 MV), and a step by step increase of the beam energy and power up to its nominal.

In the event of a major failure on the "source or accelerator" level (water leakage, arcs between electrodes, etc.), the assembly will be robotically disconnected from the bushing by cutting the cooling water tubes and by disconnecting the connectors in between the bushing and the source. The assembly will be wrapped in a sealed bag to avoid dispersing contaminated dust into the environment and will be transferred into a hot cell. The remotely controlled reassembly involves electrical reconnections and welding of water tubes; this means a complex operation and a long-term unavailability of the injector.

#### *2.7.2 Maintenance of the neutraliser and the RID*

Despite an easy access, the neutraliser and the RID, referenced to the ground potential, do not need regular maintenance (unless there is a major fault (water leakage)).

### *2.8 Conclusion*

Ultimately, this injector concept reaches its operational limits due to several limitations: a low wall-plug efficiency, a reliability lowered by heavy thermal loads and a complex 1 MV electrical setup, a difficult access to the source, accelerator and bushing leading to long operation maintenances and injector shutdowns. All these features lower the system performances and they do not really offer solutions or further adaptations to cope with the increased requirements imposed by the reactor.

## 3 Transition towards a new beamline concept for the reactors

### *3.1 Injector principle*

An injector based on modular sources referenced at the ground potential instead of a single large source at high voltage would permit easy access for regular maintenance, which is a prerequisite for the reliability and availability of the system. The source modularity would minimise the impact on the system's availability in case of failure of a source module: the injector would continue operation in a degraded mode (with the other sources modules in operation) up to the source maintenance.

The injector is divided into three parts (see the injector principle on Fig. 2):

-i) the modular part composed of sources referenced to the ground potential, each source module fixed to a 100 keV pre-accelerator.

-ii) the high voltage part composed of the +1 MV bushing which sustains and supplies the post-

 

accelerator, the neutraliser and the electrostatic residual ion deflector in the tank vacuum.

-iii) the energy recovery system collecting the residual (non neutralized) $D^-$ ions at low voltage (~50 kV).

The source "tall and narrow" aspect ratio (1.5 m long, 15 cm width) means that the beams produced are laminar. The $D^-$ beam extracted by each source module is compressed laterally and joined to a single laminar macro-beam (see Fig. 3) that is then post-accelerated up to 1 MeV in four stages (300, 500, 700 and 1000 kV). The ion beam sheet at the neutraliser's entrance is less than 5 cm wide.

There is no connection between the set "modular sources + pre-accelerator" and the high voltage assembly "post-accelerator + neutraliser+ deflector".

The topology of the extraction surface (plasma grid) interface between a "source module" and its pre-accelerator is shown in figure 4; it is composed of five grids aligned along the source axis and each one having five slits (height 25 cm, width 1 cm). The ion source has to provide a dense ($n_e$ ~$10^{18}$ $m^{-3}$) and uniform plasma column 1.5 m long to illuminate this extraction surface and produce the relevant current density $J_{D^-}$= 200 A/$m^2$; the $D^-$ current extracted would range around 12.5 A. The 3D simulation [14] of the $D^-$ beam ($J_{D^-}$=200 A/$m^2$) is shown on figure 3. The $D^-$ ions are extracted from the source by the polarisation of the pre-accelerator grids, while the co-extracted electrons are deflected out from the $D^-$ beam by permanent magnets inserted in the grids and intercepted (see paragraph 3-2).

The post-acceleration grids have large opening to minimise the interception of the macro-beam and to reduce the alignment constraints between the pre- and post-accelerator.

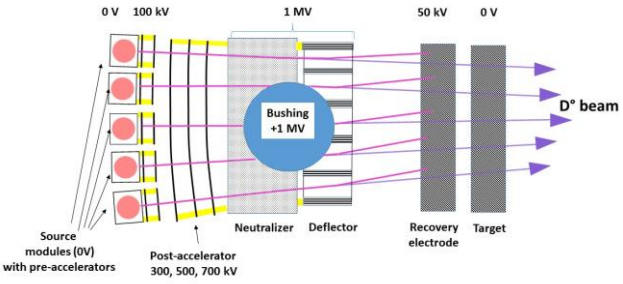


*Figure 2: Injector concept (top view) composed of five independent "source + pre-accelerator" modules, and a high voltage part composed of the bushing sustaining the post-accelerator, the neutraliser, and the electrostatic deflector. At the beamline exit, the recovery electrodes collect the non-neutralized fraction of $D^-$ at low energy (50 keV).*

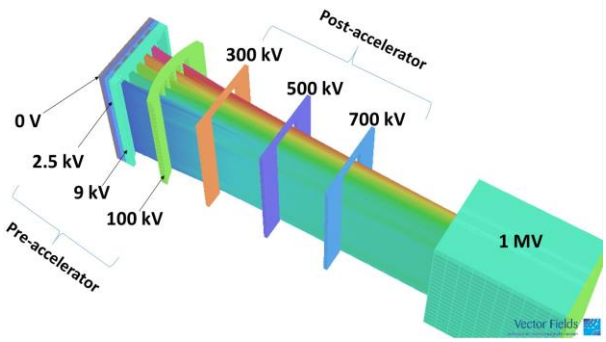


*Figure 3: 3D simulation of the $D^-$ beam in the pre and post-acceleration stages forming a single laminar beam of less than 5 cm width at the neutralizer entrance (1 MV).*

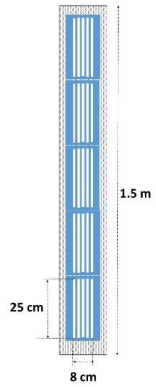


*Figure 4: Extraction surface composed of five plasma grids (PG); each grid is drilled with five slits of 25 cm height, 1 cm width.*

### *3.2 Simulation and design of the pre-accelerator*

As well as extracting and shaping the $D^-$ beam, the pre-accelerator must intercept and stop stray electrons before they reach the post-acceleration stages to avoid their acceleration and significant thermal loads downstream. Figure 5 plots the effective cross section of $D^-$ stripping as a function of the $D^-$ energy [15]. The maximum rate of stripping occurs in the extraction region (between 0 and 10 kV) where the gas density diffusing from the source is also at its maximum value. On the other hand, above 100 keV, the cross section is much lower and decreases rapidly up to 1 MeV. Consequently, the stripping rate is high in the pre-accelerator stage and low in the post accelerator due to a low stripping cross section and low gas density.

 

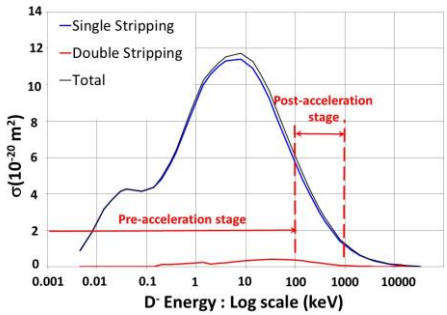


*Figure 5: Cross section of $D^-$ stripping (and double stripping) in function of $D^-$ energy.*

Figure 6 is a 2D simulation with SlacCad code [16] of a blade-like $D^-$ beamlet ($J_{D^-}$ = 200 A/m$^2$) in the pre-accelerator. The width of the slit in the plasma grid (PG) is 10 mm; the lip on the leading edge of the extraction grid (EG) enters the space of the PG to locally increase the electric field (similarly for G3.) This topology makes it possible to minimize the voltage of the grids ($V_{EG}$ = 2.5 kV, $V_{G3}$ = 9 kV). The divergence of the beam at the exit of the pre-accelerator at the level of the 100 kV grid is less than 5 mrad (see Fig. 7).

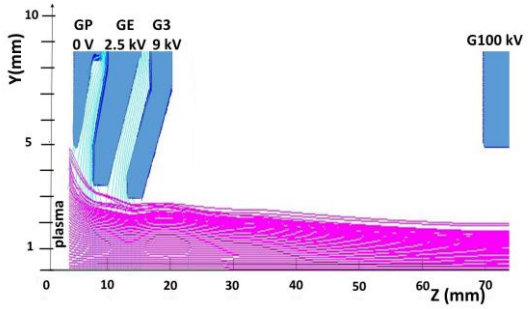


*Figure 6: 2D simulation with SlacCad code of a $D^-$ beam sheet ($J_{D^-}$ = 200 A/m$^2$) in the pre-accelerator stage*

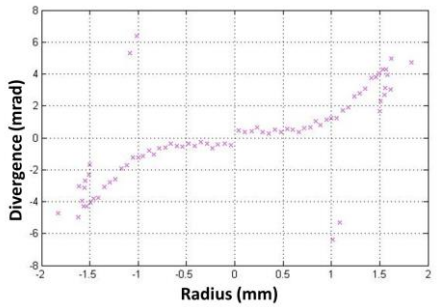


*Figure 7: Emittance diagram for the $D^-$ beamlet in the last pre-accelerator grid (G100 kV).*

To remove the electrons co-extracted (from the plasma) along with the $D^-$ ions, permanent magnets are inserted into the PG to generate locally a transverse magnetic filter in the slit aperture. The intensity of the magnetic field is in the order of 5x10$^{-2}$ T. The electrons are fully magnetised, they follow the magnetic field lines in the extraction gap (between the PG and the EG) and are intercepted by the extraction grid. A simulation of the electron 3D trajectories (see Fig. 8) results from the 2D electric field distribution of figure 6 and the 3D magnetic field map generated by the permanent magnets [17] inserted in the PG and the G3. As shown by Fig. 8 that most of the co-extracted electrons are intercepted at the EG (interception rate ~90%); the rate of leakage towards the 100 kV grid is 5%.

Due to the laminar geometry, the electrons are uniformly distributed along the slit vertical axis. This is an important distinction from the cylindrical geometry (extraction grids of the ITER type) where the co-extracted electrons are focused to a point by the lateral and vertical electrostatic lenses. The consequence is that the laminar geometry is less impacted by the co-extracted electrons current density (thermal power density on the metal grid surface), because of a lower extraction voltage ($V_{EG}$ = 2.5 kV instead of 8 kV in ITER) and of the uniform electron current distribution along the slit.

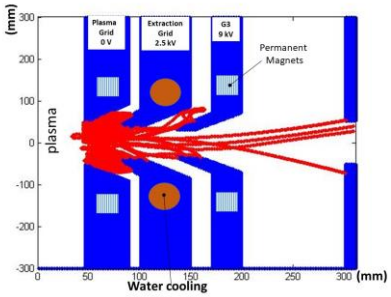


*Figure 8: 3D simulation of the co-extracted electrons trajectories in a slit channel of the pre-accelerator. Width of grid slit apertures: PG: 10 mm, EG: 8 mm, G3: 7 mm, G100kV: 10 mm.*

The electron suppression simulation of figure 8 is confirmed by the 3D simulation with the Opera code, where the $D^-$ and co-extracted electrons ($J_{D^-}$ = 200 A/m$^2$, and $J_{e^-}$ = 200 A/m$^2$) are simultaneously extracted from the plasma: the 3D electron and ion trajectories in the pre-accelerator are represented in figure 9, zoomed in the extraction gap.

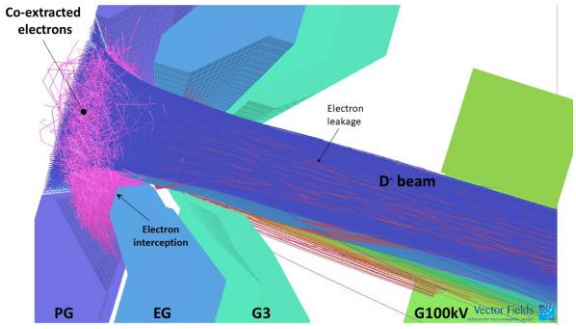


 

*Figure 9: 3D trajectory simulation (Opera 3D software [14]) of one $D^-$ beam sheet in the pre-accelerator with co-extracted electrons ($J_{e^-} = J_{D^-} = 200$ A/m$^2$). We note the electron interception at low energy (2.5 kV) on the extraction grid leading edge.*

The electron leakage for the EG and G3 grids is evaluated to 5 % of the extracted electron current.

In order to stop in the pre-accelerator stage these electron leakage and the stripped electrons emitted in the gap between the PG and the 100 kV grid (last pre-accelerator grid), permanent magnets are also inserted in the 100 kV grid. Figure 10 shows the 3D trajectories of stripped electrons emitted on the extraction grid level. We note that their interception (suppression) is complete.

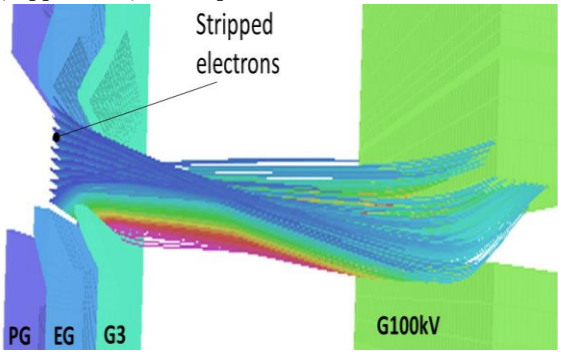


*Figure 10: 3D trajectories of stripped electrons released in the EG (2.5 kV) and G3 (9 kV) region and their deflection and suppression on the 100 kV grid.*

The magnetic filter generated by the permanent magnets inserted in the PG and the G3 is essential to remove the co-extracted electrons, but it also leads to a uniform vertical deviation of the $D^-$ ions. This divergence is compensated by the magnetic filter of the 100 kV grid which is in the opposite direction. Figure 11 shows the emittance diagram of the $D^-$ beam sheet at the pre-accelerator exit, the vertical divergence is fully compensated.

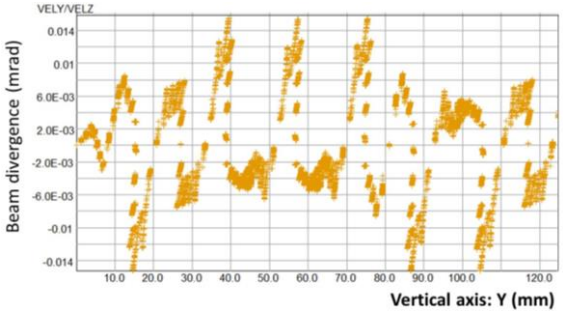


*Figure 11: Emittance diagram of the $D^-$ beam along the vertical axis downstream of the 100 kV grid. The vertical deflection induced by the transverse magnetic field of the PG is fully compensated.*

### *3.3 High voltage holding issue of the neutraliser + deflector assembly*

The "post-accelerator + neutraliser + deflector" assembly is at the high voltage (see Fig. 2). This anodic surface is surrounded by the metallic surface of the vessel (cathodic surface) at ground potential (0 V) under a high electric field ranging between 2 and 3 MV/m. This can impede high voltage holding for two reasons: first, the emission of electrons from the cathodic surface by field effect, and, second, the stored energy by the (anode-cathode) capacitance (C~ 0.5 nF):W= $\frac{1}{2}\int D.E\, dv = \frac{1}{2}$ CV$^2$ which would be released in the event of an arc. To minimize these issues, the anodic surface (exposed to the high electric field) has to be minimized.

#### *3.3.1 Electron emission issue from the cathodic surface by field effect*

The cathodic surface (vessel) emits electrons by tunnel effect resulting from the local enhancement of the electric field on micro protrusions on surfaces [18-21]. The electron current increases exponentially with voltage, and electrons are accelerated towards the anode at +1 MV; they generate X-rays, hot points, outgassing, they are likely arc precursors between the anode and the cathode.

Consequently, advanced surface conditioning protocols that tends to eliminate all types of micro-tips and pollutants on the surface are required. They must include surface "micro finishing" with Ra < 0.1 µm, the desorption of oxides and impurities (gas) from the surface by a vacuum heat treatment, and high voltage conditioning.

Due to their large surfaces, the neutraliser and the vacuum vessel will be covered with metal shields pre-conditioned by surface treatment (mirror surface + outgassing) and by high voltage conditioning in vacuum on external testbeds to sustain much higher electric fields (E > 3 MV/m) than in nominal conditions. All operations (assembly) in the vacuum vessel will take place in dust-free condition with a very high level of dust filtering.

#### *3.3.2 Energy stored in the "bushing + neutraliser + vacuum vessel" assembly*

The dimensions of a bushing for the +1 MV neutraliser are considerably reduced compared to the ITER-type bushing supplying the ion source, as a result of the smaller number of necessary cables and connectors. Indeed, the neutraliser (and the electrostatic deflector) requires only cooling water, and a voltage of 40 kV for deflecting residual ions. The 3D simulation of the "bushing + neutraliser

 

(+1MV)" assembly surrounded by a vacuum vessel (0 V) is represented in figure 12.

For this simulation, we suppose a large "neutralizer + deflector" cell (a rectangular parallelepiped of L×l×h = 3 m × 1 m × 1.5 m) surrounded by a large vessel (rectangular parallelepiped of L×l×h = 6 m, 2.5 m, 3 m). The neutraliser lies on floor insulators and is supported (and supplied) by the bushing. The equipotential surfaces are distributed in the space between the neutraliser and the vessel; the bushing is divided in four stages: 300, 500 and 700 kV and +1 MV. The total energy stored is only 150 joules; for comparison, on ITER, the stored energy in the bushing and ion source amounts to 700 joules.

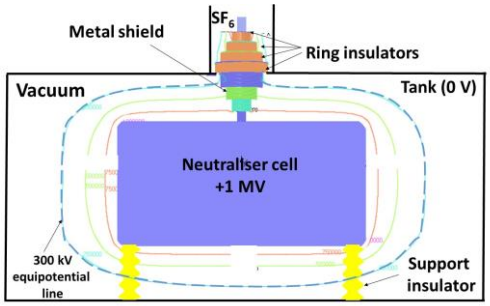


*Figure 12: Simulation of the potential distribution and stored energy in the assembly "Bushing + gas neutraliser + vessel". The neutralizer (for gas or plasma target) is 3 m long and the dimension of the vessel is: length 6 m, width 2.5 m, height 3m .*

The energy stored in the capacitance "Bushing + neutraliser + vessel" is released when a breakdown (arc) occurs between the wall of the anode (neutraliser) and the cathode (vessel). The current peak can reach several thousand amps [22-23]. It is consequently important to attenuate the current peak and to dissipate this energy by Joule effect rather than in this arc [24].

### *3.4 Beam neutralization*

#### *3.4.1 Neutralisation on a gas target*

This process is limited at 55% efficiency and requires a significant amount of gas target (the equivalent of a gas density $D_2$ : $n_{D2} \sim 4\ 10^{19}$ $m^{-3}$ over a length of three metres) to compensate the low value of the $D^-$ stripping cross section at 1 MV (see Fig. 5). This method is not compatible with the neutralizer held at the high voltage due to the long neutralizer cell (~ 3 m long), and the high water cooling flow in the deflector to damp the residual ion power.

#### *3.4.2 Neutralization by plasma target*

A plasma target of $n_e \cdot L_{neut} = 7.\ 10^{19}$ $m^{-2}$ [26] could yield a neutralization rate above 80%, but, again, the neutralizer dimension would be too large ($L_{neut}$ > 3m) to be held at high voltage.

Incidentally plasma neutralization could even raise greater difficulties than gas neutralization because the plasma density (in the neutralizer) would be ten times higher than in the ion source. As a consequence, specific and very efficient plasma confinement at the neutralizer apertures would be required to avoid any leakage of plasma and significant back-streaming of ions ($D^+$) accelerated up to 1 MeV towards the source.

#### *3.4.3 Photoneutralization*

Photo-neutralization coupled to a thin blade-like negative ion beam [27-28] simultaneously offers a complete suppression of the gas injection in the neutralizer and, potentially, an excellent beam neutralization rate. The photo-detachment cross-section has been measured to be in the range of $\sigma$ =3.6 to 4.5 $10^{-21}$ $m^2$ for $\lambda$= 1064 nm [29-30]; it gives insight into the way of designing both the beamline and its photo-neutralizer: a 1 MeV $D^-$ beam sheet of 1 cm width, a neutralization rate of 50 % requires a photon beam of 3 MW [28].

This high-power photon beam could be achieved within a high finesse (10,000) Fabry-Perot optical cavity powered by 500 W CW mono-frequency highly stabilized laser [27]. Indeed, the constructive interference at resonance which occurs between reflected waves results in a substantial enhancement (amplification) of the intra-cavity power with respect to the incoming one. The cavity is composed of four high reflectivity mirrors (mirror diameter ~10 cm) implanted on each side the ion beam sheet (see Fig. 13); the intra-cavity laser beam propagates in the same plane as the ion beam. Under this specific arrangement, the 1 MeV $D^-$ beam is crossed by four 3 MW photon beams (providing 50 % photo-detachment each) leading to a neutralization rate of 93 %; the neutralizer length is lower than 50 cm (see Fig. 13).

The photo-neutralization of a $H^-$ beam in a Fabry-Perot cavity at reduced scale was demonstrated experimentally at the Aimé Cotton Laboratory (LAC) at Orsay (France) [31]: a 1.2 keV $H^-$ beam crosses the intra-cavity 10 kW continuous wave photon beam. The cavity amplification is ~1000. It is filled with an external 10 W laser, and the photo-detachment rate amounts to ≈ 50% as expected.

 

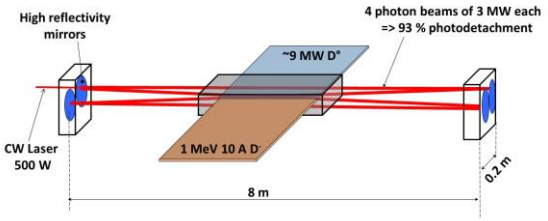


Fig. 13: Implantation of the optical cavity along a single ion beam sheet. The energetic ion beam sheet is fully overlapped and crossed by four intra-cavity photon beams of 3 MW each leading to 93% of photo-neutralization.

The photo-neutralizer concept is partially based on the Gravitational Wave (GW) detectors technology [32-34]. However there exist a major difference between the present GW detectors and a photo-neutralizer (see Table 1); indeed, while GW detectors accommodate a Fabry-Perot Michelson interferometer with a stored photon power (intra-cavity power) of 200 kW on LIGO facilities [34], a photo-neutralizer requires 3 MW of stored power. The future generation GW detectors (Einstein Telescope [35]) also targets such high photon power.

Despite the high mirror reflectivity and low photon absorption rate (~ 0.5 to 1 ppm range), the power absorbed by the mirrors (~ 1 to 3 W) under 3 MW photon flux leads to thermo-mechanical deformation [36] large enough to perturb the optical performance of the cavity. This thermal problem still requires specific studies both for the development of advanced mirrors and adaptive optics, and for compensation of the thermal distortion; the control of the mirror planarity in the nanometre range might be needed to maintain the mode stability within the cavity and minimize the intra-cavity diffraction losses.

Mitigation of the mechanical noises is another constraint in the reactor environment; it is however less stringent (see table 1) than on GW detectors which are designed to sense extremely small relative changes of the two cavity arm lengths in interference ($\delta L/L$ = 10-20 at around 100 Hz [32-34]). To avoid strong perturbations of the cavity by the mechanical noises of the reactor environment, the optical mirrors will be implanted on specific supports already used on other large highly stabilized physics instruments [37-38].

| | **GW detectors**<br>**Main achievements** | **Photo-neutralizer**<br>**Future objectives** |
|---|---|---|
| **Setup** | Two cavities in interference, common mode: frequency reference | A single cavity: frequency reference |
| **Mechanical vibration mitigation level** | $< 10^{-20}$ m $Hz^{-1/2}$ @ 100 Hz<br>(limited by fundamental noise) | $10^{-12}$ m $Hz^{-1/2}$ @ 1 kHz |
| **Stored photon power** | **200 kW** on LIGO [34] | **3 MW** |
| **Cavity** | Roundtrip: 6000 m<br>(linear cavity) | Roundtrip: 120 m<br>(ring cavity) |
| **Mirrors** | Diameter: ~35 cm<br>Planeity: < 0.5 nm RMS over Ø=15 cm<br>Roughness: < 0.1 nm RMS<br>Coating absorption: 1 ppm | Diameter: 10 cm<br>Planeity: 1 nm RMS over Ø=5 cm<br>Roughness: 0.1 nm RMS<br>Coating absorption: 1 ppm |

 

| | | |
|---|---|---|
| **External**<br>**CW Laser**<br>**(λ=1064 nm)** | Power: 350 W [39]<br>Single mode, single frequency,<br>Locked on the cavity | **Power: 500 W**<br>Single mode, single frequency,<br>Locked on the cavity |

*Table 1: Comparison of the main specifications between the GrW detectors and the photo-neutralizer. Colour code: green: available technology; red: R&D objective*

### *3.5 Recovery energy from residual ions*

As the electrical force (**F**=q **E**) is conservative, deceleration of residual ions allows conversion of their kinetic energy into electrical energy and thus increases the global efficiency of the line, no matter what neutralisation rate has been reached.

Energy recovery combined with photoneutralisation appears as the ideal solution, as the easiest to put into practice because of the absence of positive ions (residual ions at 1 MeV) at the neutraliser exit. The negative residual ions (at 1 MeV) are deflected at the exit of the neutraliser and collected by the recovery electrode at a low voltage (~50 kV) (see Fig. 14), and the recovered current is returned to the current circulating in the 1 MV source (see Fig. 15). The only role of the electrostatic deflector is to deflect the residual $D^-$ beam towards the recovery electrode. As it does not collect any ion, the thermal load is low.

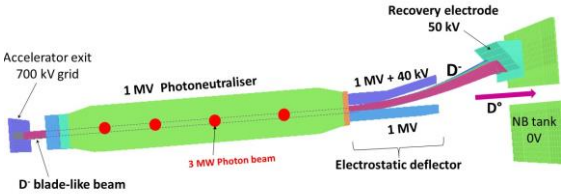


*Figure 14: 3D simulation of the 1 MeV $D^-$ trajectories at the neutralizer exit: electrostatic deflection and collection on the recovery at low voltage (50 kV).*

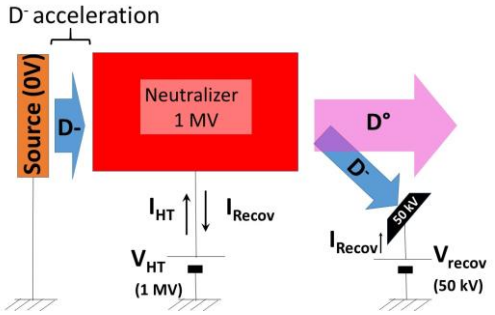


*Figure 15: Principle of the electrical setup for the $D^-$ beam energy recovery with grounded source (and neutralizer at 1MV).*

### *3.6 Injector efficiency*

Attaining high efficiency and reliability of neutral beamlines requires a significant reduction in the amount of gas along the beamline by minimising the gas conductances.

The gas distribution was calculated under the assumption that the injector is composed of five beamlines operating in parallel, with 11 A of $D^-$ per line providing 55 A of $D^-$ (same ion current as the ITER injector).

As the stripping losses mainly occur within the pre-accelerator stage, it is clear that an ion source operating at very low pressure would significantly reduce the negative ions losses and stray particles ($e^-$, $D^+$, $D^0$) in the pre-accelerator. Figure 16 shows a comparison of the gas pressure distribution along the blade-like accelerator for an injector with five sources with gas neutralizer or photoneutralizer. Figure 17 shows the corresponding relative $D^-$ beam intensity (100 % of $D^-$ at the source level) for these two configurations. With a photoneutralizer, the negative ion losses amounts to 14 % mainly in the pre-accelerator with less than 1 % in the post-accelerator stage

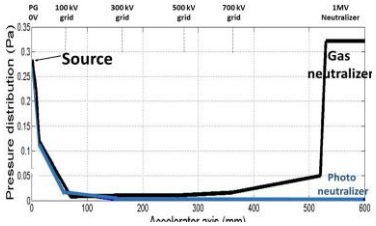


*Figure 16: Pressure distribution in the accelerator cavity; Black : Injector with gas neutralizer; Blue: Injector with photo neutralizer.*

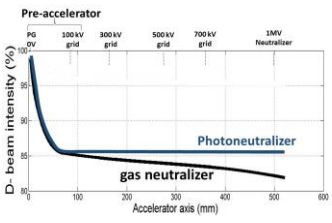


 

*Figure 17: Comparison of the $D^-$ beam relative intensity (%) in the accelerator ; Black curve: gas (or plasma) neutralizer; Blue curve: Photo neutralizer.*

The wall plug efficiency is evaluated using the same references as for the ITER injector:
Same current of $D^-$ extracted (55 A in total which is 11 A per source)
Same power supplies :
-i) 1 MV power supply: 60 A, 95% electrical efficiency, that is 3 MW of losses
-ii) Ion source power supply: 800 kW of RF power (that is 160 kW per source)
Electric power for the pumps (pumping and water-refrigeration): 1 MW

The power loss by the $D^-$ stripping in the pre-accelerator is evaluated to 0.8 MW, it is lower than 0.1 MW in the post-accelerator.
Level of neutral particle beam losses in the duct by re-ionisation and interception: ~15%

If we assume a neutralisation rate of 90% for photoneutralization (with 3 MW of photon power stored in each cavity), the wall plug efficiency ranges around 74%, the injector would couple a neutral beam of 40 MW in the plasma core.

A photoneutralization-based injector offers definitely the best performances: simplification of the beamline and high voltage setup, very little stripping losses in the accelerator ⇔ low thermal loads in the accelerator, no gas and no plasma in the neutraliser, and very low thermal loads on the neutralizer and deflector cells (=> small bushing).

.

### *3.7 Additional advantages of a photoneutralization based neutral beam system with recovery energy*

#### *3.7.1 Control of neutral power deposition in the plasma*

The neutralization rate and the photon power in the optical cavity are proportional to the external CW laser power supplying the cavity: $P_{cavity} = P_{Laser}$ x S, with S = Power enhancement factor of the cavity, and $P_{Laser}$ the external CW laser power.

Consequently, the neutral power of each blade beam can be tuned only by varying the external laser power. The remaining 1 MeV non-neutralized fraction of negative ions ($D^-$) are collected at low energy (~50 keV) onto the cooled recovery electrode, even with a low photo-neutralization rate (high $D^-$ current).

In the horizontal direction (equatorial plane), it is equally possible to modulate the power deposition in the plasma if the extraction grid supports ($V_{Eg}$ = 2.5 kV et $V_3$ = 9 kV) of the pre-accelerator are divided into two segments electrically insulated from each other and connected to independent power supplies and fast switches (tetrodes or static interrupters). This allows the switching off/on of each half blade of the beam in the micro-second range.

Equipped with these two features, it would be possible to couple and modulate the power deposition of neutral particles at each part of the toroidal plane to control the plasma profile.

#### *3.7.2 Conditioning of the injector on the target*

In the conditioning phase, it is the beam target which intercepts and diagnoses the $D^0$ beam. At full neutral power, the target panels cannot sustain the huge heat load. To limit the power density to less than 2 MW/m$^2$ on the panels, the CW laser power (supplying the cavity) is reduced for a low photodetachment rate, and the energy recovery will collect the $D^-$ ion beam at low energy. As the photoneutralization process changes the beam optics in a negligible way, the low power $D^0$ beam on the target brings back information on the ion beam (1 MeV $D^-$) optics that enters the photoneutralizer.

Consequently, the recovery electrode will be designed for a high thermal load of more than 40 A of $D^-$ beam at 50 keV, i.e., 400 kW per blade beam.

## 4 Design and maintenance of a photoneutralization-based neutral beam system for reactors

### *4.1 Design and maintenance of the "source + pre-accelerator" assembly*

With the 1 MV bushing sustaining the photoneutralizer in the tank vacuum, the optical cavities and ion beams are in the horizontal plane (see Fig. 18 and 19).

The injector is made up of four sets: (1) the "source + pre-accelerator" modules, (2) the high voltage assembly (see Fig. 20) comprising the 1 MV bushing which sustains and supplies under vacuum the set "post-accelerator, neutralizer cell, electrostatic deflector", (3) the recovery electrode (~50 kV) and beam target referenced to the ground, and, (4) the optical tanks (with the cavity mirrors) located on both sides of the vessel.

The ion source being referenced to the ground potential, all source and pre-accelerator connections (water, gas, electricity, caesium oven, high voltage supplying the pre-accelerator) are positioned at the rear of the vacuum tank (see Fig. 18). The

 

connectors are fixed on bellows permitting horizontal translation so that the connections can be remotely connected (or disconnected) from the source under vacuum by telemanipulation. The water-cooling system is connected by helicoflex joints, whose water tightness is provided by the joint ring (Helicoflex) compressed by the external fixation of the bellows.

### *4.2 Caesium management*

To produce the required $D^-$ current density in the plasma, caesium is injected in the plasma source. In a reactor, the long term operation leads to a significant consumption, between 0.5 and 1 kg of caesium per year. As a consequence, the caesium oven has to be regularly filled and migration of caesium outside the source (towards the acceleration stages) is a real issue when deposited on the accelerator grids and lowering the grid surface work function. That degrades the HV holding (arc between grids) of the accelerator and produces stray $D^-$ (under the $D^0$ grid bombardment of the caesiated grids), resulting in an aberrant ion beam which bombards the grids downstream (increase of the thermal loads).

On ITER, the source being suspended under vacuum by the bushing, the access to the caesium oven by remote handling is not so straightforward. To replace the caesium oven, the operation is made in air; it requires injector shut down.

With the ion source referenced to the ground, access to the caesium ovens by remote handling is easy; it doesn't require any injector shutdown as it can be replaced directly from the rear flange of the vacuum vessel without breaking the tank vacuum.

In addition, the caesium diffusing from the plasma source downstream in the pre-accelerator is, for the major part, trapped on the actively cooled pre-accelerator grids (EG, G3 and G100 kV) due to the narrow slit apertures.

To keep the injector availability, the caesium polluted assembly (source module+ pre-accelerator) has to be regularly extracted from the injector tank and replaced by another clean and pre-conditioned assembly (with a full caesium oven) keeping the injector under vacuum conditions.

The maintenance of each "source + pre-accelerator" module is done without breaking the vacuum to avoid the injector deconditioning. For that purpose, each module can slide on rails in a support (see Fig. 21) which makes its transfer into an external container and easy removal possible (see Fig. 22). The container is equipped with a vacuum valve. It is designed to be fixed to the vacuum valve on the vessel positioned on the source level. The two vacuum valves will be opened when the two vessels are under vacuum.

After the module has been extracted from the injector and the valves closed, the container (containing the module under vacuum) will be removed, evacuated via the evacuation chamber (see Fig. 18) and placed in a hot cell outside the plant. The used source module can be replaced immediately (using the inverse procedure) by another module under vacuum in a container that is already prepared and conditioned for use.

To cope with these constraints, the source module aspect ratio is long and thin, it is designed to produce a dense and uniform plasma column illuminating the caesiated extraction grid (see Fig. 4). A helicon plasma driver such as developed at SPC-EPFL laboratory [40, 41] is up to now the best candidate to fulfil these requirements.

### *4.3 Design and maintenance of the high voltage assembly*

4.3.1 The photoneutraliser cell

It is a rectangular parallelepiped (less than 50 cm long) crossed by the ion and photon beams. It is supplied and maintained under vacuum by the 1 MV bushing on the top (see Fig. 20); the thermal load on the neutralizer is low, it only results from the interception of the remaining stray particles and stripped electrons.

4.3.2 The post-accelerator

The accelerator grids are fixed and aligned to the neutraliser cell by insulators in the top and bottom (see Fig. 19-20). These insulators are protected from parasitic particles from the beam by the chicanes of the grid supports. There is neither a chicane nor an isolator on the lateral sides of the grid supports, to allow an efficient gas pumping on both sides. To keep the alignment with the pre-accelerator stage, the 300 kV stage of the post-accelerator rests on insulators fixed on the reference support of the injector (see Fig. 19). Each stage of the post-accelerator is supplied (water and high voltage) by metallic tubes coming from the bushing.

4.3.3 The electrostatic deflector

It is equally fixed to the neutraliser by 50 kV isolators. It is also supplied with water and high voltage by the bushing. With a photoneutraliser, there are no $D^+$ residual ions, and the thermal load on the deflector is also low.

4.3.4 The Bushing

Due to the likely aging of insulators resulting from radiations (X-rays, neutrons), the bushing will have to be replaced by a new one after a few years of operations (around 3 to 5 years). Extraction of

 

the complete high voltage assembly (see Fig. 20) comprising "the post accelerator, the neutraliser, the deflector and the bushing" will require the shutdown of the injector. The complete assembly can be removed by the crane, placed in a dedicated container for evacuation into a hot cell and replaced by a new one (already conditioned on external testbed and ready for use).

4.3.5 Design and maintenance of the optical cavities

The proposed solution which is presently under investigation is the use of folded optical Fabry-Perot cavities with a finesse of a few thousand which are fed with a 500W highly stabilized external laser. To fully overlap the blade-like ion beam of 2 cm width in the interaction region, the intra-cavity photon beam diameter in the interaction region has to be close to 2 cm Full Width Half Maximum (FWHM) leading to a long cavity. To make cavity integration in the reaction environment easy, the cavity optical length has to be as short as possible. On the other hand, the optical tank containing the mirrors under high vacuum must be located within the bioshield, a few metres away from the injector tank. Using of a telescope [42] makes it possible to reduce the cavity optical length to 30 m without any additional cavity stability perturbations. As a result, the distance between opposite mirror can be only 8 m (see Fig. 23).

As the optical components of the cavities (mirrors, laser) are fragile and sensitive to fouling, they must be placed in tanks under high vacuum far away from the injector to avoid stray particles, pollutants (oxides) and radiations. They are located outside the nuclear island (see Fig. 18), sheltered in a bunker. To mitigate mechanical vibrations, they are mounted on active and passive vibration isolators [37-38]. The photon beams propagate in pipes connecting the injector vessel to the optical tanks. Vacuum valves installed between the injector vessel and the pipes (see Fig. 23) allow maintenance of the optical components by telemanipulation without vacuum break of the injector vessel.

 

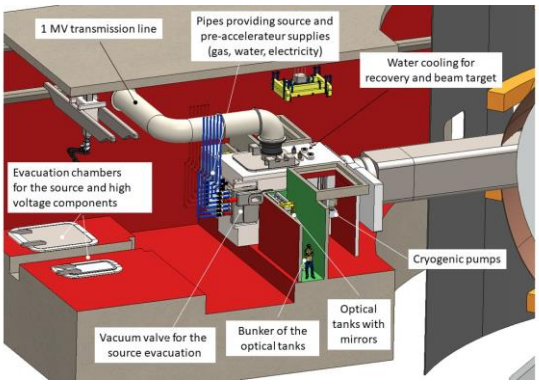


*Figure 18: Overview of the injector in the hall; we note that the optical tanks with mirrors and lasers are implanted behind walls in a bunker (shieldings) to protect them against the harsh nuclear environment and to favour the access for their maintenance.*

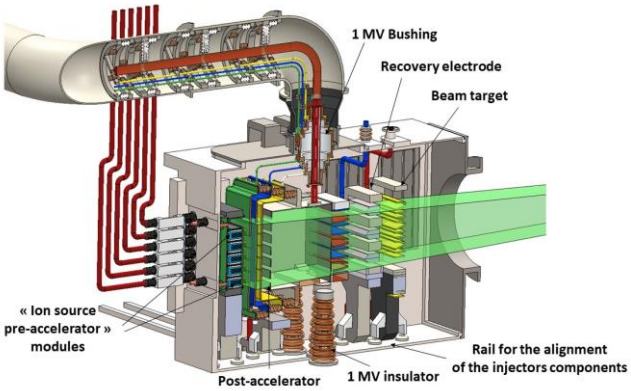


*Figure 19: Vertical cross section of the injector. The injector components (source, accelerator, recovery and target) are fixed on a reference support to ensure the beam alignment. The ion sources are in the horizontal plane to provide horizontal laminar ion beams. The set "ion sources + pre-accelerator" are maintained in a support referenced to the ground potential. The set "post-accelerator+neutralizer cell + deflector" is maintained and powered by the 1 MV bushing. This high voltage assembly lies on 1 MV insulators fixed on the reference support to keep the beamline alignment.*

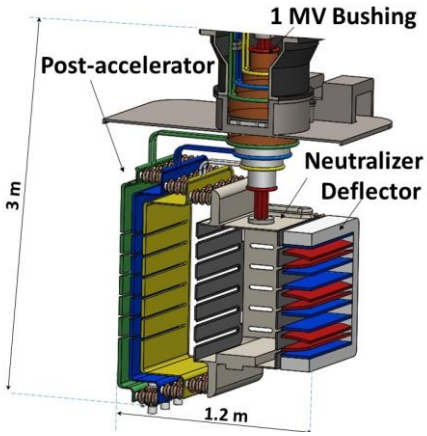


*Figure 20: High voltage assembly comprising the bushing, the post-accelerator, the neutralizer and deflector.*

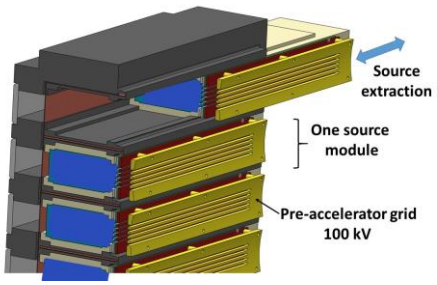


*Figure 21: Zoom of the "ion source + pre-accelerator" modules in their support. The modules are fixed on a slide for their extraction (maintenance). They are supplied from the rear face of the vacuum vessel.*

 

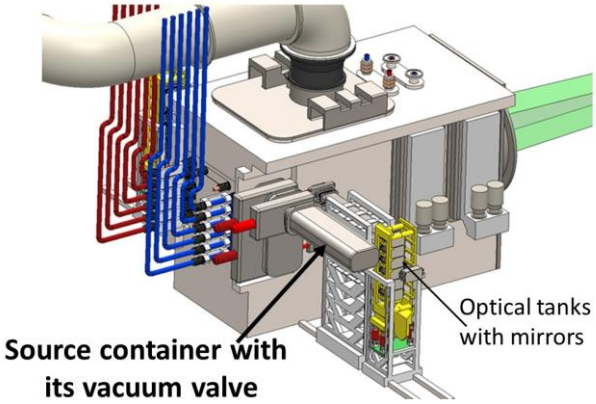


*Figure 22: Source maintenance: principle of the source module extraction in the container.*

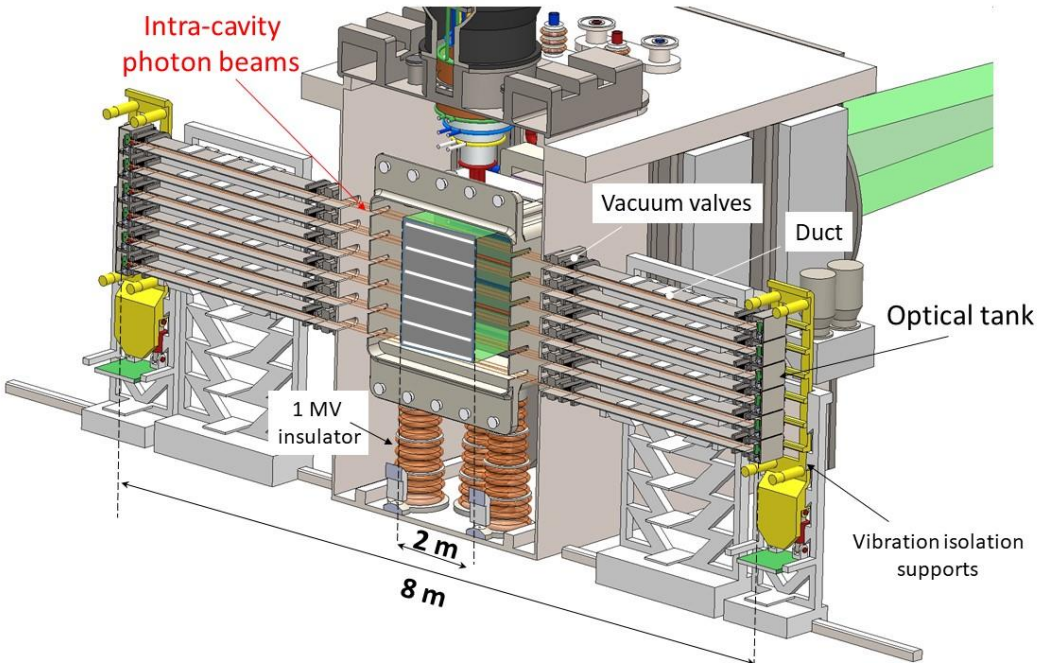


*Figure 23: Injector cross section on the photoneutralizer region.*

 

## Conclusion

In addition to nuclear safety constraints aiming to avoid exposure and contamination of workers by using remote control handling, achievement of an economic fusion reactor with electricity production at low cost imposes a high level of unprecedented requirements for the heating systems. The challenge is to develop high power heating systems (~ 100 MW of power coupled in the plasma core) with very high wall-plug efficiency (above 60 %) able to operate in reliable and stable conditions over long term operations (several months).

In view of these new challenges, the question arises of the compatibility of current systems and their ability to adapt to these new reactor requirements:

-i) the negative ion source is the complex and active component of the injector that requires a regular maintenance. However, on current systems, the source is held to the high voltage (-1 MV), the electrical setup at -1 MV supplying the RF source is complex, invasive, difficult to access, complicating the maintenance operations of the source. The risk of failure is significant, and the system availability raises questions.

-ii) the injector wall plug efficiency is low; it only ranges around 30 % due to several limitations: a neutralization by gas target lower than 55 %, significant beam losses and thermal loads in the accelerator (evaluated to ~10 MW), no energy recovery system for the energetic residual ions, which, in addition, produce heavy thermal loads (~16 MW) on the residual ion dump. Implementation of an energy recovery system would increase the complexity of the electrical setup and beamline, which would make the injector reliability even lower.

From the evidence that this injector concept does not really offer solutions or further adaptations to cope with the increased RAMI requirements and nuclear safety imposed by the reactor, it is clear that a new concept breaking away from the conventional systems has to be addressed.

An injector concept with modular sources at ground voltage, which provides blade-like beams to reduce the gas load (beam losses), is proposed. The assembly is devised such that each source and its pre-accelerator can be replaced by a new one without breaking the vacuum and affecting the injector conditioning. To maintain a high availability of the injector, the new source and its caesium oven have been pre-conditioned on an external testbed and ready-for-use.

The main issue of an injector with sources at ground potential is the anodic surface composed of the neutraliser and deflector at high positive voltage, surrounded by a large cathodic surface (the metallic wall of the tank). This concept stands if the anodic surface can be minimised and if electron field emission by the cathodic surface is maintained to an acceptable level by advanced conditioning protocols including ultra-high vacuum techniques, super-fine surface states, and the elimination of dust. Neutralisation by plasma target, which could potentially attain a 80% neutralization rate, cannot be considered for several reasons: the large anodic surface ("neutraliser + RID" length of 5 m), high thermal loads due to residual 1 MeV D+ ions on the RID, and the plasma confinement issue at the neutralizer apertures.

Other neutralization concepts have been explored worldwide over the last decades, such as the neutralization by metal foils, by other gas, by alkali metal vapor jets [43], or, beam-beam neutralization [44]. All of them have faced major issues, such as additional pollution, increase of the beam divergence and complexity; they have not been considered as reactor relevant.

With a much smaller anodic surface and very low thermal loads on the neutralizer cell and deflector, photoneutralization remains the only route for an injector with grounded source. Associated with energy recovery from residual $D^-$ ions, the system will attain unprecedented injector performances: very high neutral power for plasma heating and current drive, high wall-plug efficiency, low thermal loads, unprecedented capabilities for temporal and spatial modulation of the neutral beam deposition in the plasma to control the stability. In addition, the grounded ion source and the optical tanks located in bunkers make it possible to fulfill the RAMI and nuclear safety requirements by providing easy and rapid access by telemanipulation without affecting the reactor availability. The other injector components (the "high voltage assembly") do not need regular maintenance; it will take place during the reactor shutdowns.

Up to now, the photoneutralization feasibility studies already carried out on reduced scale prototypes have not highlighted any showstoppers. The next step to overcome in the years to come is the implementation of a full-scale high power cavity prototype in the 1 MW range and the achievement of a thin blade-like $D^-$ beam, possibly provided by a helicon based ion source.

 

## Acknowledgements

This work has also been carried out within the framework of the EUROfusion Consortium and has received funding from the European Union's Horizon 2020 research and innovation programme under grant agreement number 633053. The views and opinions expressed herein do not necessarily reflect those of the European Commission.

The authors are very grateful for fruitful scientific collaborations around neutral beam systems with the Swiss Plasma Center team (EPFL, Lausanne, Switzerland) and in France, with S. Bechu (LPSC laboratory, Grenoble), G. Cartry (PIIM laboratory, Marseille), and G. Fubiani (Laplace laboratory, Toulouse) , as well as for their advices in preparing this manuscript.

## References

[1] Federici G, Biel W, Gilbert M.R 2017 Nucl. Fusion 57, 092002

[2] Stork D et al 2017 Nucl. Fusion 57, 092001

[3] Federici G, Boccaccini L & Cismondi F 2019, Fusion Engineering and Design 141, 30-42

[4] Grisolia C et al. 2019 Nucl. Fusion, 59, 82019

[5] Zohm H, Träuble F Biel W 2017, Nucl. Fusion 57, 086002

[6] Pamela J, Bécoulet A & Borba D 2009 Fusion Eng. Des. 84, 194

[7] Hemsworth R S et al. 2017 New J. Phys. 19, 025005

[8] Watanabe K et al. 2009 Nucl. Fusion 49, 055022

[9] Tobari H et al. 2017 IEEE Transactions on plasma science 45, n° 1, p162

[10] Heinemann B et al. 2017 New J. Phys. 19, 015001

[11] De-Esch H et al. 2015 Nucl. Fusion 55, Number 9

[12] Fubiani G et al. 2008 Physical Review Special Topics – Accelerators and beams- 11, 014202.

[13] Hopf C et al. 2019 Fusion Eng. Des. 146, Part A, 705-708

[14] Opera 3D; Vector Fields Limited; 24 Bankside Kidlington; Oxford OX5 1JE, England

[15] Barnett C, "Atomic data for fusion " Vol. 1; ORNL—6086/V1, DE91 000527.

[16] Pamela J 1991 Rev. Sci. Instrum. 62, Issue 5 10.1063/1.1141995

[17] Ciric D Private communication

[18] Latham R (Ed.) Academic Press, Aston University, Birmingham, UK, 1981, ISBN 0-2-437175-2

[19] Anders A – Cathodic arcs. Springer Science (2008).

[20] Seznec B et al. 2017 Phys. Rev. Accel. Beams, 20, 073501

[21] Simonin A et al. 2013 Fusion Eng. Des. 88, 1–7

[22] Villecroze F et al. 2013 Fusion Eng. Des. 88, Issues 6–8, p. 891

[23] Pesce A De Lorenzi A Consorzio RFX, 35127 Padova (Italy), RFX ref: RFX NBTF TN 59.

[24] Ahmed K De-Esch H Simonin A 2019 IEEE Transactions on Plasma Science, Volume: 47, Issue: 3.

[25] Pesce A De Lorenzi A Boldrin M 2011 Fusion Eng. Des. 86, Issues 6–8, p. 847

[26] Surrey E Holmes A 2013 AIP Conference Proc. 1515, 532 https://doi.org/10.1063/1.4792825

[27] Chaibi W et al. 2009 AIP conference proceedings, ISBN 978-0-7354-0630-8, p385.

[28] Simonin A et al. 2015 Nucl. Fusion 55, 123020

[29] O'Connor A.P. et al. 2015 Rev. Sci. Instrum. 86, 113306.

[30] Vandevraye M et al. 2014 Phys. Rev. A 90, 013411.

[31] Bresteau D, Blondel C & Drag C 2017 Rev. Sci. Instrum. 88, 113103

[32] Abbott B. P. et al. 2016 Phys. Rev. Lett. 116, 241103

[33] Aasi, J et al. arXiv, e-print. [ADS], arXiv:1304.0670v1 [gr-qc] 2 Apr 2013

[34] Haocun Yu et al. Nature 2020 583, 43–47

[35] Punturo M et al. 2010 Classical Quant. Grav. 27, 194002.

[36] Fiorucci D Feng J Pichot M Chaibi W 2015 AIP Conference Proceedings, ISBN 978-0-7354-1297-2, 050010.

[37] Moshrefi M et al. 2012 J. Sound Vib. 331, 1532-1541.

[38] Balik G Caron B Allibe J Badel A 2013 J. of Intelligent Material Systems and Structures 24(15) p1785

[39] Dixneuf C et al. 2020 Optics Express, Vol. 28, Issue 8, p10960

[40] Furno I et al. 2017 EPJ Web of Conferences 157, 03014 (2017); DOI:10.1051/epjconf/201715703014.

[41] Marini C et al. 2017 Nucl. Fusion 57 036024

[42] Fiorucci D, Hreidi A & Chaibi W 2018 Appl. Optics B122 Vol. 57, No. 7 / 1 March 2018 /

[43] Grisham L 2007 Phys. Plasmas 14, 102509.

[44] Hicks N Wong A 2007 J. Fusion Energ. 26, Nos. 1/2, DOI: 10.1007/s10894-006-9039-0